Double gradient multilayers for broadband focusing

Christian Morawe*[a], Jean-Christophe Peffen[a]
Eric M. Dufresne[b], Yong S. Chu[c], Albert T. Macrander[c]

[a]European Synchrotron Radiation Facility, BP 220, F-38043, Grenoble Cedex, France
[b]Dept. of Physics, The University of Michigan, Ann Arbor MI, 48109, USA
[c]Advanced Photon Source, Argonne National Laboratory, Argonne, IL, USA

ABSTRACT

We have designed and fabricated a new type of focusing multilayer mirror, capable of reflecting a divergent beam over a large energy band around 9 keV. A flat energy response about 10% wide and providing a reflectivity of 50% has been achieved by a non-periodic bi-layer sequence while a lateral thickness gradient follows the varying Bragg condition over the whole mirror length. The focusing setup is based on a simple one-point bender and a pre-shaped substrate. A focal spot size of about 8 micrometers has been obtained at a distance of 285 mm from the center of the mirror using synchrotron radiation from an undulator source. Energy dependent scans have shown that this device enables focusing experiments with fixed geometry at variable energies.

Keywords: Multilayers, focusing, depth gradient, x-ray optics, synchrotron radiation

1. INTRODUCTION

A useful way to illustrate the overall performance of reflecting optics in the hard x-ray regime around 8keV is to plot the integrated reflectivity versus the intrinsic energy bandwidth of each device as shown in Fig.1. The graph is divided into two sectors separated by a diagonal line indicating the ideal peak reflectivity of 100%. The triangle above this line is therefore a naturally “forbidden area”. Below this line we find gray zones representing familiar x-ray optical elements ordered as a function of their energy resolution: from perfect single crystals on the left, over multilayers in the middle, to total reflection mirrors and filters to the right. Some data points are added for particular elements. Diamond symbols represent perfect single crystals (values taken from [1]). Squares indicate experimental data from multilayers prepared at ESRF. One essential message one can deduce from this graph is the tremendous potential gain in flux when going from highly resolving crystals to multilayers or mirrors. The second is the existence of open areas between the three traditional families of devices.

The gap between single crystals and multilayers could be filled-up by distorted crystals [2]. However, coherence preservation has become an important issue at 3rd generation synchrotron sources, limiting somehow the use of these elements. Recently, the development of weakly absorbing, high-resolution multilayers on super-polished substrates has helped to overcome this obstacle [3-6].

The open zone between traditional multilayers and mirror-filter combinations can be bridged by non-periodic layered structures. First attempts to apply such structures in short wavelength radiation concerned the design of supermirrors for neutron beams [7]. This concept was then extended to hard x-rays [8]. The main obstacle is to find a layer sequence that provides the required, mostly broad and smooth reflectivity spectrum. A more recent approach consists in the use of analytical calculations to obtain approximate solutions for the layer thickness dependence that are then optimized by numerical algorithms [9]. This technique is able to design various given reflectivity spectra both energy and angle-dependent and in a reasonable amount of time. Consequently, depth-graded structures have been developed and fabricated to fulfil the Bragg condition either for fixed incident angle and varying energy or vice versa [10, 11].

Focusing or collimating multilayer optics generally require a lateral thickness gradient to account for the variation of the incident angle [12, 13] given by the focusing geometry. Thanks to the bigger angle of incidence, they provide an up to four times larger beam acceptance as compared to total reflection mirrors, but with the drawback of their limited energy bandwidth.

* Correspondence: Email: morawe@esrf.fr; Telephone: xx33-4-7688-2588; Fax: xx33-4-7688-2325

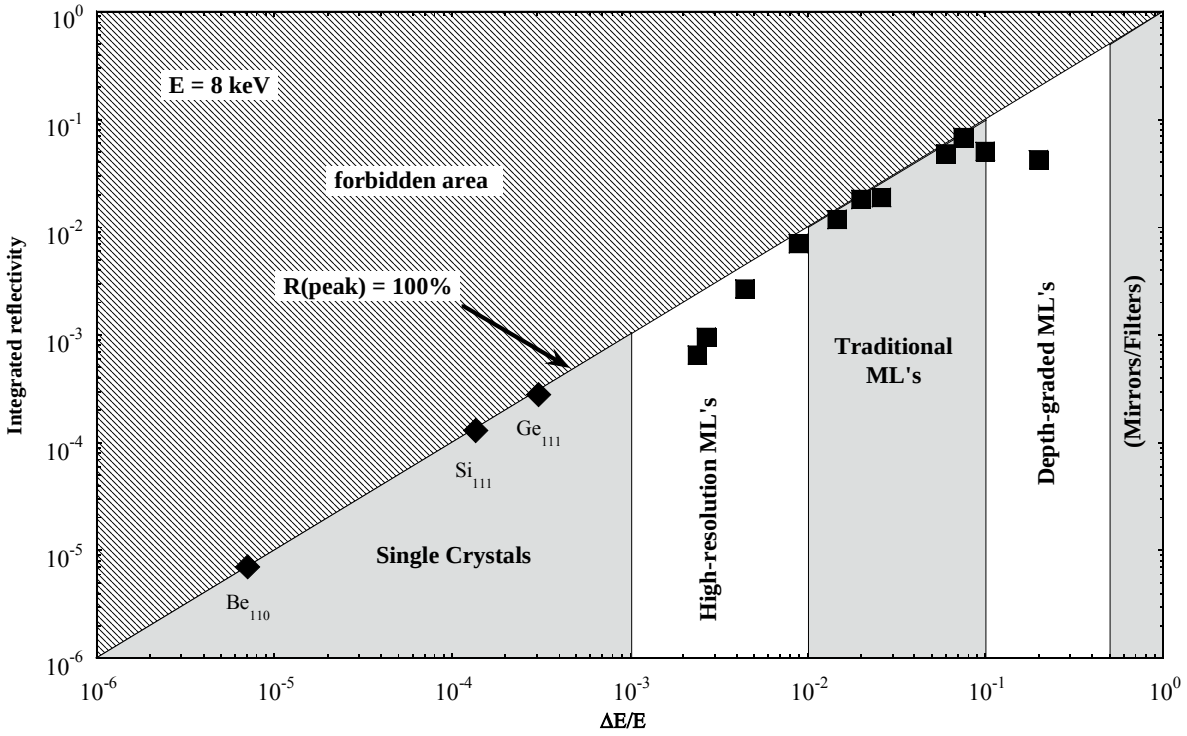

Fig.1: Integrated reflectivity versus energy bandwidth of reflecting optical elements at 8keV. Only the triangle below the limiting diagonal line corresponding to a peak reflectivity of 100% is physically relevant. The shaded area is therefore naturally "forbidden". Gray zones indicate familiar elements such as single crystals, multilayers, and total reflection mirrors. Diamond symbols represent perfect single crystals, squares show experimental data of various multilayers produced at ESRF.

The next step would be to merge the two techniques of lateral and depth gradient into one device, that is, depositing a multilayer with a lateral thickness gradient to account for the varying Bragg condition along the mirror, and adding a depth gradient to increase the energy bandwidth. This would allow the design of a focusing mirror with fixed focal distance and large beam acceptance over a reasonably wide energy range.

The concept is illustrated in Fig.2 and is similar to that of DuMond diagrams [14]. In the energy dispersion equation

$$E = \frac{h \cdot c}{2 \cdot \Lambda \cdot \sqrt{n^2 - \cos^2 \theta}} \ , \tag{1}$$

the angular dependence has to be interpreted in terms of the distance f from the position on the mirror to the focal spot, that is $\theta=\theta(f)$. Here, h is the Planck constant, c the speed of light in vacuum, Λ the multilayer period, n the average complex optical index in the multilayer, and θ the grazing angle of incidence. Equation (1) represents Bragg's law including a refraction correction. In the case of a parabolic mirror, we have

$$\sin^2 \theta = \frac{p}{2 \cdot f} \ . \tag{2}$$

The corresponding geometry is illustrated in Fig.3. Here, p defines the opening of the parabola by

$$2 \cdot p \cdot x = y^2 \ . \tag{3}$$

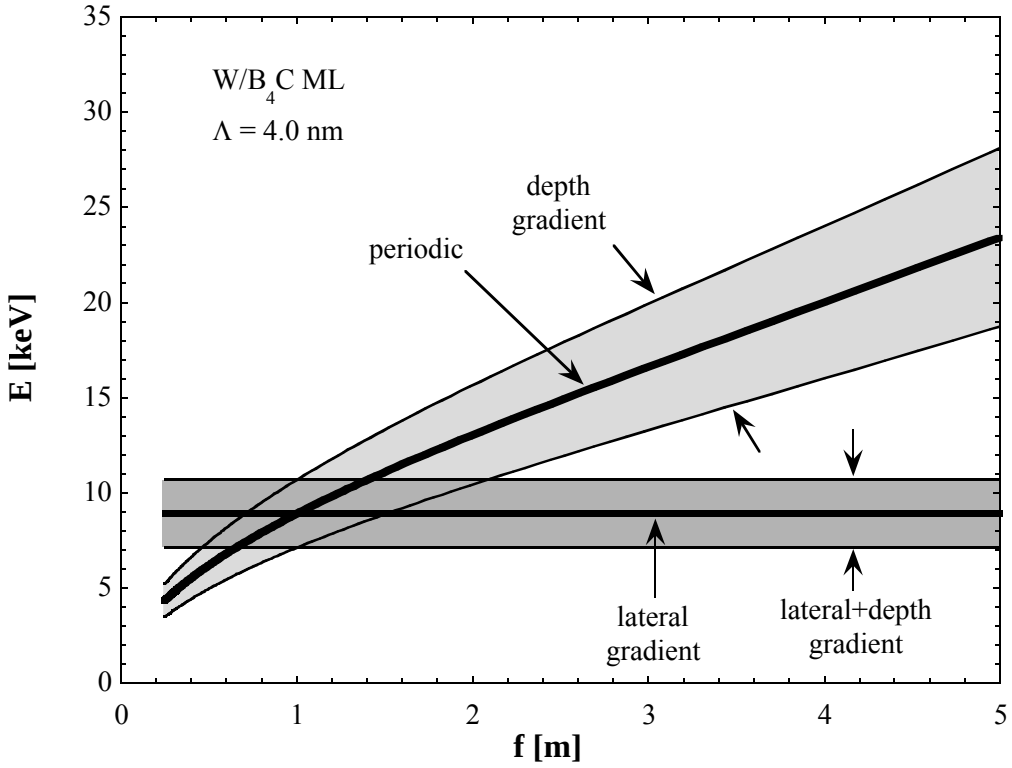

Fig.2: Energy dispersion of different types of multilayers. The plot shows the reflected energy E versus the distance f from the focal spot along the multilayer surface. Thick solid lines represent periodic multilayers either with or without lateral thickness gradient. A purely depth-graded non-periodic multilayer covers the zone shaded in light gray. A combination of lateral and depth gradient is indicated by the area colored in dark gray.

One can therefore plot the locally reflected energy or energy interval versus the distance f from the focal spot along the multilayer surface.

A periodic multilayer without lateral gradient is characterized by the curved thick solid line in Fig.2. Such a structure reflects x rays only in a narrow "intersection volume" of (E,f) space, defined by the intrinsic multilayer line width of typically a few percent. If one adds a lateral period thickness gradient, the energy response becomes constant (horizontal solid line). In practice, this has the advantage that the multilayer reflects at the same energy over the whole mirror length. A non-periodic multilayer without lateral gradient widens the energy band pass and therefore opens the dispersion area from the curved solid line to the zone in light gray, thereby increasing the intersection zone in (E,f) space. The most attractive solution, however, is a combination of lateral and depth gradient. Such a multilayer is characterized by the dark gray rectangular area in Fig.2. It provides a broad and constant energy bandwidth over its whole length.

In this work we have designed and fabricated a focusing multilayer mirror based on a simple bending device and a pre-shaped substrate [13]. It is meant as a proof of feasibility for the combination of lateral and vertical thickness gradient in multilayers.

2. MULTILAYER DESIGN

Several aspects have to be taken into account during the design phase of a double-graded multilayer. The lateral thickness gradient has to match the variation of the Bragg angle caused by the curvature of the mirror within the chosen focusing geometry sketched out in Fig.3. In the present case, the mirror shape is parabolic with a focal distance of f=285mm and an angle of incidence of θ=0.93º, given with respect to the center of the mirror. For synchrotron applications with a source distance of the order of q=50m, the incoming beam is sufficiently parallel to justify the use of a parabolic shape. The multilayer has an active length of 270mm leading to a maximum beam acceptance of 4.5mm in the plane of incidence. The useful width of the coating is about 10mm. The design of the lateral d-spacing variation was done for a mean energy of 9keV. W and B_4C were chosen as coating materials due to the strong optical contrast in this energy range. Fig.4 shows the d-spacing Λ of the multilayer along the total active length of the mirror indicating the steep lateral gradient necessary to reflect the x rays at every point of the mirror. The ratio Γ=t(W)/Λ was kept constant throughout the multilayer to facilitate the following steps of the design.

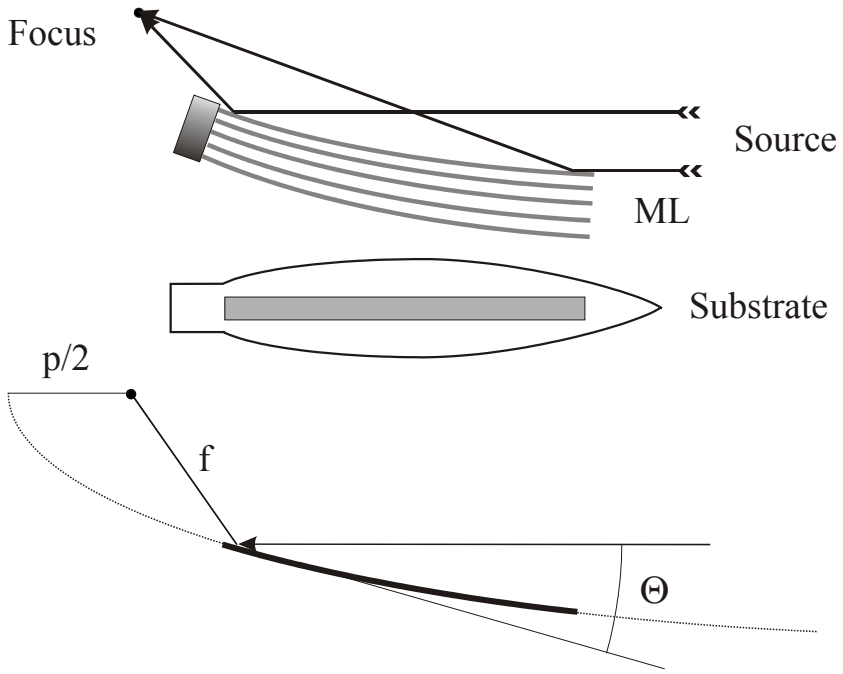

Fig.3: Focusing geometry of the parabolic multilayer mirror. Due to the long distance to the source the incoming x rays can be approximated as parallel. The substrate is clamped at the left side and pushed by a screw near its tip. The d-spacing increases from the left to the right due to the decreasing angle of incidence.

The additional thickness variation with depth was added using the center of the mirror as a reference. The goal was to enlarge the intrinsic bandwidth of 4-5% FWHM of a periodic W/B_4C multilayer to about 9% and to provide a flat plateau with a constant reflectivity of 50%. Fig.5 shows the layer sequence after the optimization procedure. The period thickness oscillates between 3.5nm and 5.0nm with only slight variations near the top of the stack. To avoid surface modifications of the structure after exposure to air, a B_4C cap layer was added in the design.

Fig.6 shows the reflectivity as a function of energy corresponding to the layer structure in Fig.5. The design goal is indicated as a horizontal line. No effort was made to suppress the reflectivity outside of the optimization region between 8.6keV and 9.4keV. 40 periods were chosen to obtain the required performance. A purely numerical refinement routine based on a least square fit algorithm was applied. A periodic multilayer with a d-spacing of 4.0nm was used as a starting point for the refinement.

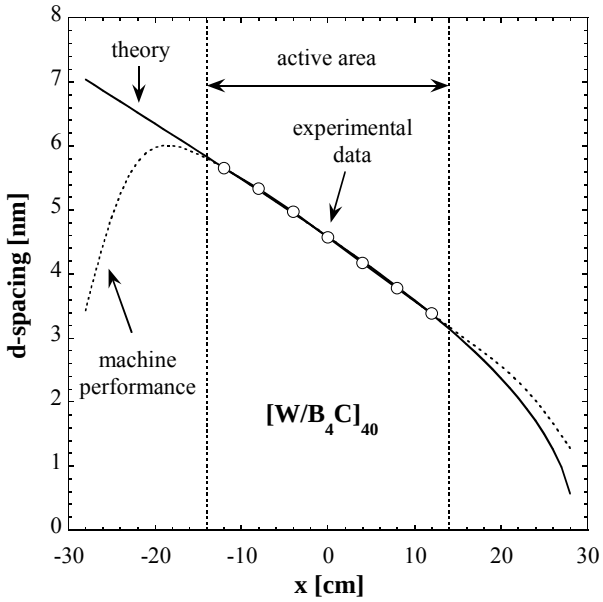

Fig.4: W/B_4C multilayer d-spacing along the total length of the mirror following the required lateral gradient. The solid line is the ideal curve obtained from geometrical and optical considerations. The broken line takes into account the realistic performance of the coating facility. Open circles show experimental data points derived from x-ray reflectivity scans.

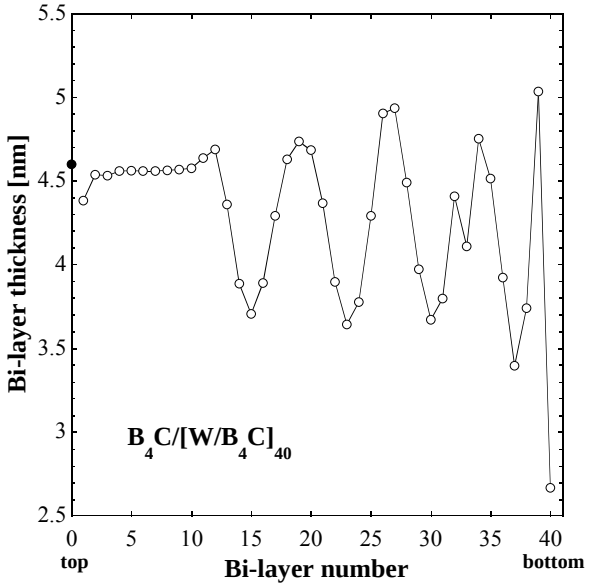

Fig.5: Bi-layer thickness versus bi-layer number at the center of the W/B_4C multilayer as obtained from numerical optimization (open circles). A protecting B_4C layer is indicated separately (solid circle). The line is a guide to the eye

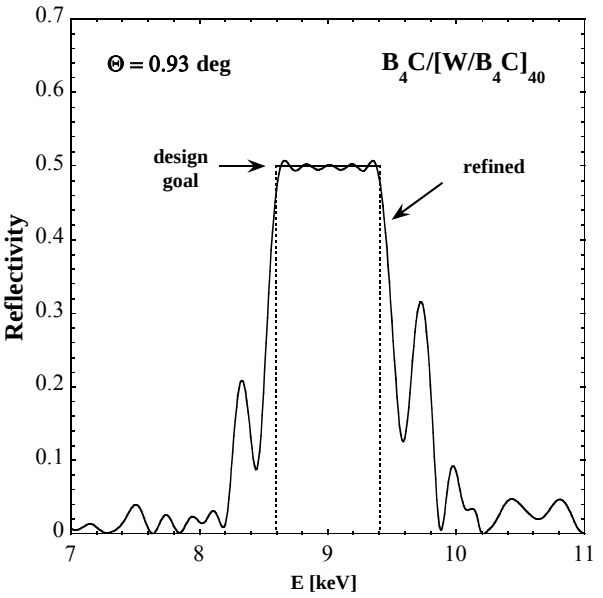

Fig.6: Calculated reflectivity (solid line) at the center of the optimized non-periodic W/B_4C multilayer. The design goal (box function) is indicated as a horizontal line.

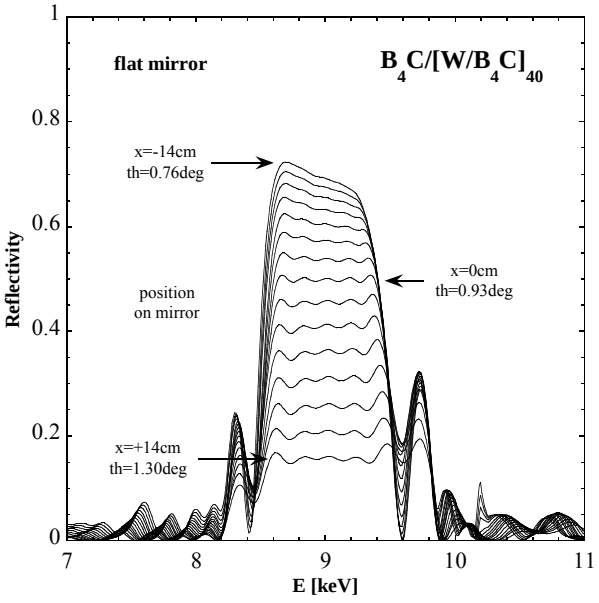

Fig.7: Calculated local reflectivity at different positions on the flat multilayer varying from -14cm (top curve) to +14cm (bottom curve) with respect to the center.

To estimate the performance of the total curved multilayer, some more steps have to be carried out. Since the d-spacing varies along the multilayer the reflectivity spectra will not be exactly the same everywhere. Fig.7 is a compilation of local reflectivity spectra of the flat multilayer calculated for different positions from -14cm to +14cm in intervals of 2cm with respect to the center of the sample. It is evident that, due to the decreasing d-spacing and the increasing angle of incidence θ, the overall reflectivity decreases when going from -14cm to +14cm. In addition, since the penetration depth varies as well, the shape of the curves change qualitatively. Here, the limits of the present approach using independent optimization procedures for lateral and depth gradient become visible. At this point the geometrical influence on the flux density of the curved mirror has to be taken into account. When a uniform parallel beam hits a parabolic mirror (Fig.3) as defined in equations (2) and (3) the local flux density reflected to the focal spot from a given solid angle around an incident angle θ(f) is given by

$$I(\theta) \approx R(\theta) \cdot f(\theta) \approx R(\theta) \cdot \frac{p}{\sin^2 \theta} \ . \qquad (4)$$

The series of curves in Fig.7 representing R(θ(f)) therefore have to be multiplied by the last term in equation (4). The result is plotted in Fig.8. The intensity variation is more emphasized due to the effect described above. Nevertheless, as long as the total flux in the focal spot remains the main interest, the θ-dependence does not play an important role. As shown in Fig.9, the average intensity profile versus energy remains rather flat (to be compared with Fig.6), despite the influence of the local multilayer reflectivity and the geometrical effect of the curvature.

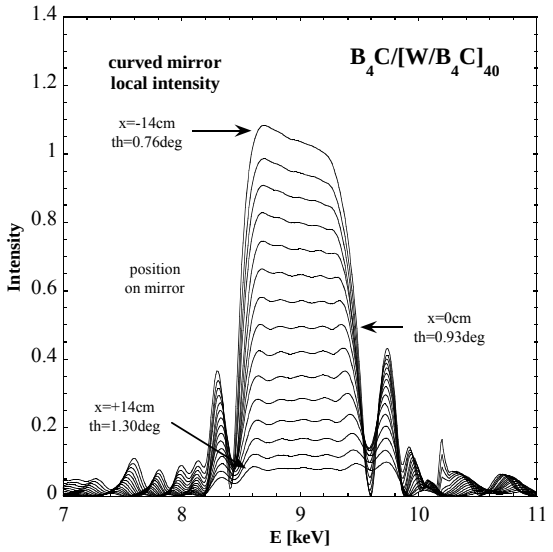

Fig.8: Local intensity (flux density) after reflection from different points on the curved multilayer. The respective curves correspond to those in Fig.7.

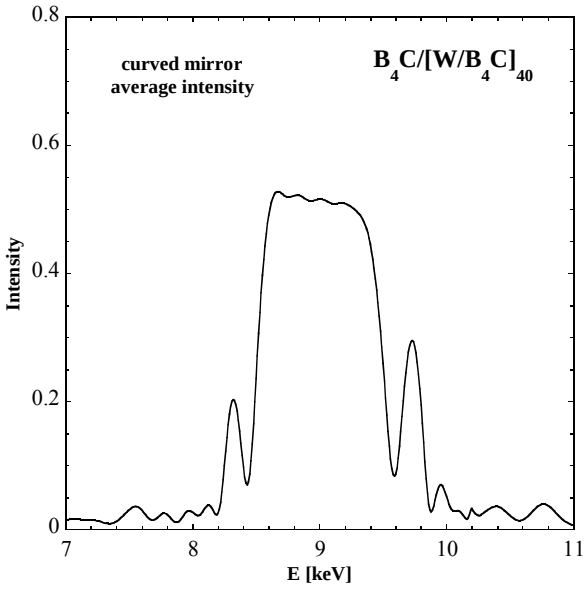

Fig.9: Average intensity at the focal spot after reflection from the whole curved multilayer.

3. DEPOSITION TECHNIQUE

The multilayers were deposited by Distributed Electron Cyclotron Resonance (DECR) sputtering [15]. The Ar plasma was maintained at p(Ar)=1.3·10^{-3}mbar. The W and the compound B_4C target were polarized with –800V and –1950V DC, respectively, leading to deposition rates of R(W)=0.09nm/s and R(B_4C)=0.03nm/s. The coatings discussed here were done in a dynamic mode, where the targets are moved with a well-defined speed profile underneath the substrate. The irregular layer stacking as shown in Fig.5 was obtained using a data table that modifies the speed profiles from one period to the next. As mentioned in section 2, the relative speed distribution and therefore the lateral gradient is the same for all layers. Only the total average speed and accordingly the mean thickness changes from layer to layer. All other coating parameters were

kept constant during the process. The final coatings for the bent mirror were done on pre-shaped glass substrates. Equivalent depositions were made for reference purpose on flat Si substrates.

4. CHARACTERIZATION

The samples were characterized by θ:2θ X-ray reflectivity scans taken on a fixed anode reflectometer at E=8048eV followed by numerical simulation of the data. Fig.10 gives an example of two measured curves, one at the center of the multilayer deposited on the pre-shaped but flat glass substrate (circles), and one of a reference sample on a flat Si substrate (squares) with respective numerical fits (solid lines). For comparison, the dashed line indicates the design goal.

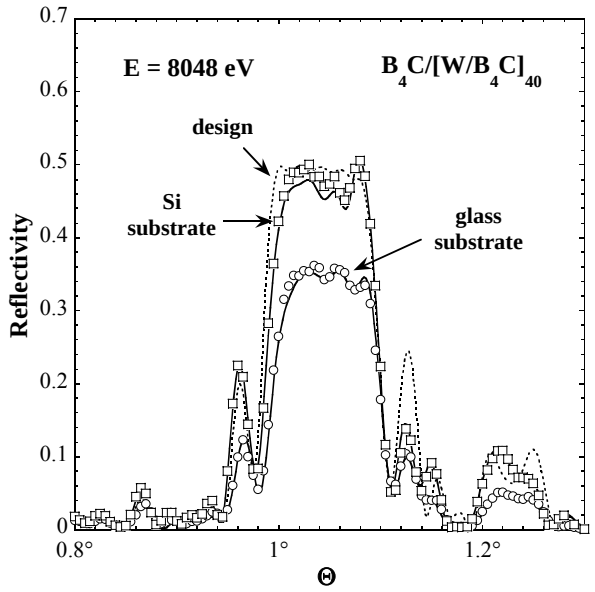

Fig.10: Experimental reflectivity data of two equivalent flat multilayers. Circles are data of a coating on a glass substrate, squares those from a deposition on a Si substrate. The solid lines are numerical fits to the data. The dashed line corresponds to the original design.

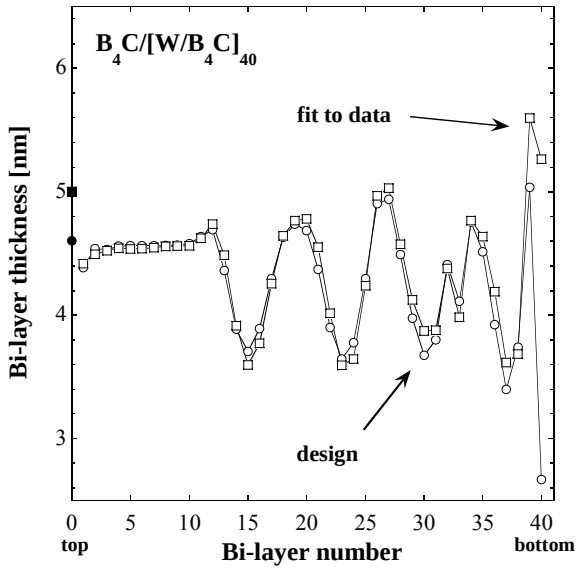

Fig.11: Bi-layer thickness versus bi-layer number of the W/B_4C multilayer coated on a Si substrate (squares) after numerical refinement compared to the design goal (circles). Protecting B_4C layers are indicated separately (solid symbols).

Both curves show a broad peak with a width of about 0.1° corresponding to an energy bandwidth of 10% and a well-pronounced plateau. The peak reflectivity, however, differs between 35% for the multilayer on glass and almost 50% for the one on Si. It is known from former studies [13] that the glass substrates utilized here do not have a surface finish comparable with state-of-the-art Si substrates as used for the reference sample in Fig.10. This difference in substrate quality explains the loss in reflectivity for the multilayer on glass. The undulations on the reflectivity plateau as well as some variations in the fringes around the peak can be attributed to minor thickness modifications at the top and the bottom of the multilayer stack, as shown in Fig.11. The plot shows the layer sequence for the coating on Si (open squares) compared to the ideal structure (open circles). The B_4C cap layer is added using solid squares and circles, respectively. When using high quality Si substrates, the overall agreement in structure and reflectivity response between design and experiment is remarkable.

In order to verify the lateral thickness gradient, the multilayer was measured at different positions from -12cm to +12cm with respect to the center. The derived period thickness is plotted in Fig.4 as open circles on top of the theoretical curves. The mean error between experiment and design is below 1%. Since the multilayer under study is non-periodic, “period thickness” means here a reference value representing the entire stack. No relative thickness variations between layers were allowed during this operation.

Fig.12 gives an impression of the evolution of the local reflectivity as one scans along the flat multilayer mirror from -12cm to +12cm. As discussed in section 2, shape and intensity of the profiles change as the angle of incidence changes. Since this characterization was done on a monochromatic laboratory source, no energy dependent spectra as shown in Fig.7 could be measured. The unexpected drop in reflectivity for the curve at -12cm is caused by the reduced reflecting area near the tip of the substrate. Nevertheless, the qualitative similarity of the curves in Fig.7 and Fig.12 is obvious.

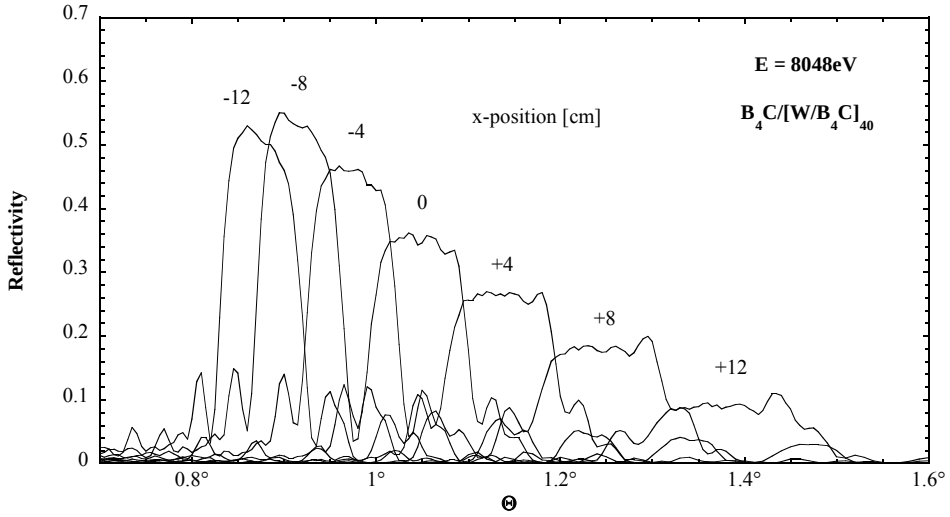

Fig.12: x-ray reflectivity curves measured at various positions from -12cm to +12cm along the flat multilayer mirror. -12cm corresponds to the zone near the tip of the substrate as indicated in Fig.3.

5. FOCUSING EXPERIMENTS

The above-characterized multilayer was mounted on a simple bending device as indicated in Fig.3. The setup is explained in more detail in [13]. Focusing experiments were carried out at the Advanced Photon Source (APS) on the undulator beamline 7ID (MHATT-CAT). In order to image the focused beam, a lens-coupled CCD with 1k x 1k pixels was used, in which the visible light produced by the x-rays striking the scintillator is magnified by an objective lens and detected by the CCD. The camera head was protected against external light by a 25μm thick Al foil. The effective pixel resolution for the experiment using 5x objective magnification was 1.34μm. The point spread function of the scintillator was determined to about S_{PSF}=2μm. The CCD system was mounted on a detector arm of a six-circle Kappa diffractometer and the distance from the center of the multilayer to the scintillator of the CCD was set to be 285mm. An ion chamber was placed 157cm upstream from the multilayer to monitor the primary intensity. The beam was reflected and focused horizontally. The curvature of the multilayer was pre-set on the optical Long-Trace-Profiler (LTP) of the APS Metrology Laboratory and then in-situ refined using x rays and the CCD camera. Several series of scans were taken with fixed focusing geometry while varying the photon energy of the incoming beam. This was achieved by simultaneously moving the undulator gap and following with the fixed exit double Si crystal monochromator [16].

Fig.13 shows an image of the focal line at 9.1keV when the multilayer was exposed with the maximum available beam size, which is 1.5mm in the horizontal and 1.0mm in the vertical direction, as defined by slits. Under these conditions a section of about 70mm of the multilayer is illuminated. Fig.14 shows a cross section through the focal line after integration over 5 central pixel rows to improve the signal-to-noise ratio. From a Gaussian fit to the data one extracts a full width at half maximum (FWHM) of the focal line of about S_{EXP}=8μm. This value corresponds roughly to the results obtained earlier using a similar substrate on the same bending device [13]. With a source distance of 54m and a focal distance of 285mm, one obtains a geometrical demagnification of 0.00528. Since the horizontal source size (FWHM) is about 830μm, one would expect a source limited line width of S_S=4.4μm. The measured figure error of the flat mirror contributes to about S_{FE}=4.0μm to the total line width. Adding the squares of all relevant sources of line broadening, one obtains a theoretical estimate of S_{TH}=6.3μm which represents a lower limit compared to the measured 8μm.

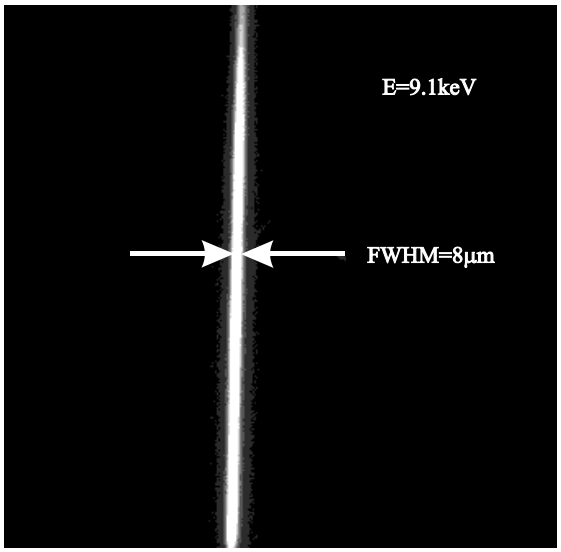

Fig.13: CCD image of the focal line at 9.1keV and at 285mm from the center of the multilayer. The size of the incoming beam was 1.5mm (horizontal) and 1.0mm (vertical).

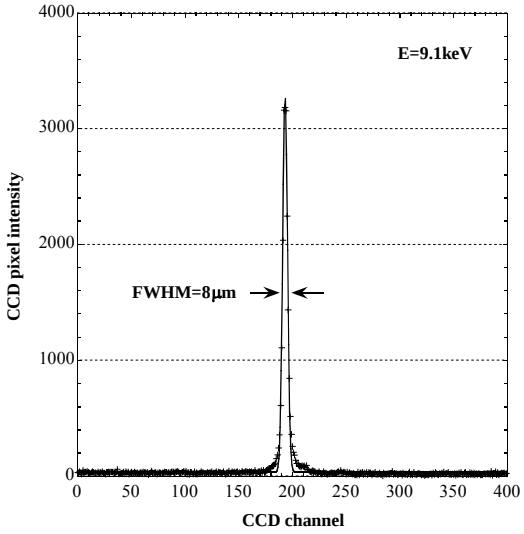

Fig.14: Cross section through the focal line shown in Fig.13. To improve the signal-to-noise ratio, the intensity was averaged over 5 central pixel rows. The experimental data (+) has been fitted by a Gaussian function.

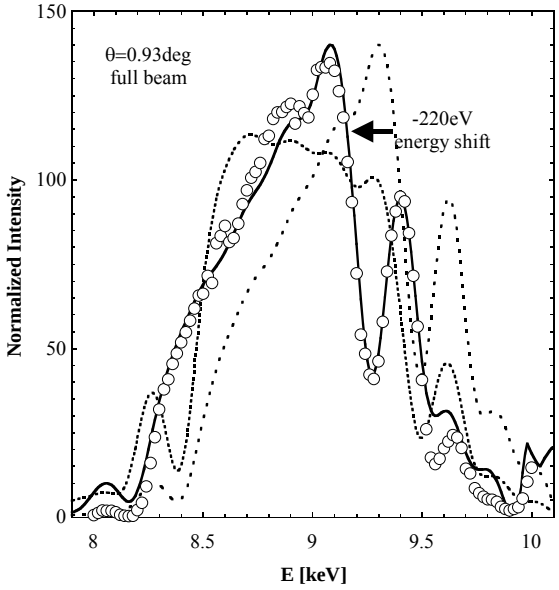

Fig.15: Normalized total intensity of the focal line measured on the CCD detector (circles) versus photon energy. The background was removed. The dashed line indicates the ideal spectrum, the solid line is the result after corrections due to absorption and energy offset.

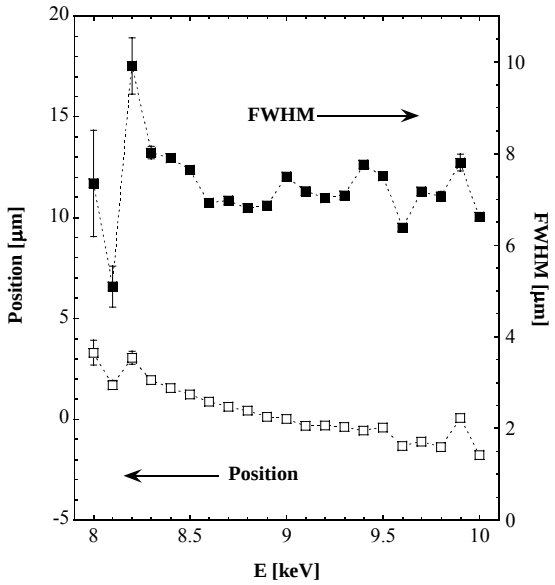

Fig.16: Focal position (open squares) and FWHM (full squares) of a series of cross sections as indicated in Fig.14. All values have been derived from Gaussian fits to the respective data.

The main goal of this experiment was, however, to test the focusing performance as a function of energy. In Fig.15 the measured total intensity (circles) of the focal line is plotted versus the photon energy. Comparing the data with the expected spectrum as obtained from simulations (dashed line) as presented in Fig.10, a clear disagreement in shape and position can be observed. To understand this difference, some details of the experimental setup have to be considered. Between the CCD camera and the ion chamber, that detects the reference intensity, the x-ray beam is attenuated by air. The Al window of the CCD and additional Al absorbers enhance this effect. Since the absorption of x-rays in matter is energy dependent, a correction has to be applied to the expected intensity distribution. The scintillator response is roughly proportional to the photon energy, which has to be taken into account. In addition, small errors during the sample alignment cannot be excluded, since the mirror was curved and since the multilayer reflection is rather broad. A rough analysis of the alignment procedure shows that errors up to 500eV in energy may have occured due to errors in θ and in the impact point of the beam.

If one takes into account a total air path of 185cm and 0.25mm of Al, and if one allows for an energy offset of -220eV due to misalignment, one obtains a simulation as indicated by the solid line in Fig.15. All main features of the measured data can be reproduced. The principal effect of the absorption correction is a strong intensity reduction at lower energies. Although the derivation contains several experimental parameters, the good agreement between experiment and theory is quite convincing.

Besides the total intensity, the stability of the focal line was an important issue under study. In Fig.16 the position and the FWHM of the focus are plotted as a function of the photon energy. All values have been derived from Gaussian fits to the respective data sets. It can be seen that, within the error margin, the FWHM is approximately constant between 7 and 8μm, in good agreement with the above estimate of the line width. The position of the focal line moves only slightly by about 5μm, which gives a good measure of the reliability of the whole experimental setup including the incoming beam.

6. DISCUSSION

The focusing experiments have shown that the double-graded multilayer performs approximately as expected from the characterization done beforehand. Special care has to be taken on the experimental conditions, in particular during the sample alignment and on the monitoring of the total intensity.

The size of the focal line is clearly limited by the moderate substrate quality and by the relatively simple bending device. An improvement of the focal spot would be straight forward using one of the ESRF state-of-the-art bending devices [17] equipped with a substrate with low figure error. Given a sufficiently small virtual source size, focal spots below 1μm would then be possible [18].

In the present case, the high absorption, the steep lateral gradient and, in a similar manner, the strong geometrical effect on the local flux density, provoke a huge intensity variation along the curved multilayer. This means a challenging task for the design of the depth gradient. The latter remains, in the present approach, qualitatively the same at all positions on the substrate. As a consequence, the spectra change in shape and intensity as the angle of incidence and therefore the penetration depth of the beam into the multilayer increase. Theoretically, one could design optimized non-periodic layer sequences at various points on the mirror, separated from each other by a finite lateral distance. This, however, could lead to completely different solutions for neighbouring zones and therefore to non-continuous lateral thickness profiles which, in turn, would be in conflict with the need for a smooth lateral gradient. A global optimization algorithm would have to be developed, capable of optimizing simultaneously the lateral and the vertical thickness profiles within the multilayer.
Most applications on 3rd generation synchrotron beamlines, however, require less severe boundary conditions than those discussed above. Photon energies above 10keV and less pronounced lateral gradients significantly reduce the mentioned drawbacks on the performance leaving enough space for devices using double-graded multilayers.

7. SUMMARY

It has been shown that the combination of lateral and vertical thickness variations in multilayered structures is feasible from a theoretical as well as from a practical point of view. Based on a simple focusing setup, a multilayer based focusing device has been designed, fabricated, and tested. It provides a fixed focusing geometry while offering a broad and flat energy response of about 10%. It therefore unifies the advantage of the wide energy range of a total reflection mirror with the increased angle of incidence of a multilayer. Further efforts will be made to integrate such a device into ESRF beamline optics.

ACKNOWLEDGMENTS

The authors would like to thank Amparo Rommeveaux from the ESRF Optics Group and Lahsen Assoufid from the APS Optics Group for their cooperation on the metrology measurements and Dohn Arms and Petr Ilinsky from MHATT-CAT for their participation during the focusing experiment.
Use of the Advanced Photon Source was supported by the U.S. Department of Energy, Basic Energy Sciences, Office of Science, under Contract No. W-31-109-Eng-38.

REFERENCES

1. A. K. Freund, "Synchrotron x-ray beam optics", *Proc. 6th Summer School on "Complementarity between neutron and synchrotron x-ray scattering"*, Zouz, Switzerland, ed. A. Furrer, 329, (1998).
2. K.-D. Liss, A. Magerl, "Can a gradient crystal compete with a mosaic crystal as a monochromator in neutron- or x-ray diffraction?", *Nucl. Instr. And Meth. A* **338**, 90 (1994).
3. Ch. Morawe, J-Ch. Peffen, E. Ziegler, A. K. Freund, "High resolution Al_2O_3/B_4C multilayers", *Proc. SPIE* **4501**, 127 (2001).
4. A. Baranov, R. Dietsch, Th. Holz, M. Menzel, D. Weißbach, R. Scholz, V. Melov, J. Schreiber, "High resolution Carbon/Carbon multilayers", *Proc. SPIE* **4782** (2002).
5. T.W. Barbee, R. A. London, R. L. Shepherd, V. N. Shlyaptsev, A. Wootton, "Multilayers for the soft x-ray and x-ray spectral domains", *Proc. SPIE* **4500** (2001).
6. V. Martynov, Y. Platonov, A. Kazimirov, "High selective x-ray multilayer mirrors for monochromatization and spectroscopy", these Proceedings (paper 5195-8).
7. P. Høghøj, E. Ziegler, J. Susini, A. K. Freund, K. D. Joensen, P. Gorenstein, J. Wood, "Broad-band focusing of hard x-rays using a supermirror", *Nucl. Instr. and Meth. B* **132**, 528 (1997).
8. F. E. Christensen, A. Hornstrup, N. J. Westergaard, J. Schnoper, J. Wood, K. Parker, *Proc. SPIE* **1546**, 160 (1992).
9. I. V. Kozhevnikov, I.N. Bukreeva, E. Ziegler, "Design of x-ray supermirrors", *Nucl. Instr. and Meth. A* **460**, 424 (2001).
10. V. V. Protopopov, "Graded x-ray multilayer optics for laboratory-based applications", *Proc. SPIE* **4144**, 116 (2000).
11. Ch. Morawe, E. Ziegler, J.-Ch. Peffen, I. V. Kozhevnikov, "Design and fabrication of depth-graded x-ray multilayers", *Nucl. Instr. and Meth. A* **493**, 189, (2002).
12. M. Schuster, H. Göbel, L. Brügemann, D. Bahr, F. Burgäzy, C. Michaelsen, M. Störmer, P. Ricardo, R. Dietsch, T. Holz, H. Mai, "Laterally graded multilayer optics for x-ray analytics", *Proc. SPIE* **3767**, 183 (1999).
13. Ch. Morawe, P. Pecci, J. Ch. Peffen, E. Ziegler, "Design and performance of graded multilayers as focusing elements for x-ray optics", *Rev. Sci. Instrum.* **70**, 3227 (1999).
14. J. W. M. DuMond, *Phys. Rev.* **52**, 872 (1937).
15. M. Pichot, J. Pelletier, in *Microwave Exited Plasmas*, edited by M. Moisan and J. Pelletier, (Elsevier, Amsterdam, 1992).
16. E. M. Dufresne, D. A. Arms, S. B. Dierker, R. Clarke, Y. Yacoby, J. Pitney, B. MacHarrie, R. Pindak, "Design and performance of a stable first crystal mount for a cryogenically cooled Si monochromator at the Advanced Photon Source", *Rev. Sci. Instrum.* **73**, 1511, (2002).
17. O. Hignette, P. Cloetens, W.-K. Lee, W. Ludwig, G. Rostaing, "Hard x-ray microscopy with reflecting mirrors: status and perspectives of the ESRF technology", *J. Phys. IV* **104**, 231 (2003).
18. P. Coetens, O. Hignette, W. Ludwig, S. Bohic, E. Pereiro, Ch. Morawe, "Hard x-ray phase contrast microscopy and fluorescence mapping with KB optics", accepted for publication in *Proc. SRI* (2003).